CrossMark

ORIGINAL PAPER

# Earthquake hazard and risk assessment based on unified scaling law for earthquakes: Altai–Sayan Region

Vladimir G. Kossobokov[1,2,3] · Anastasia K. Nekrasova[1]

**Abstract** We apply the general concept of seismic risk analysis based on morphostructural analysis of the territory, pattern recognition of earthquake-prone nodes, and the Unified Scaling Law for Earthquakes, USLE, in another seismic region of Russia to the west from Lake Baikal, i.e., Altai–Sayan Region. The USLE generalizes the empirical Gutenberg–Richter relationship making use of apparently fractal distribution of earthquake sources of different size: $\log_{10} N(M, L) = A + B \cdot (5 - M) + C \cdot \log_{10} L$, where $N(M, L)$ is the expected annual number of earthquakes of a certain magnitude $M$ within an seismically prone area of linear dimension $L$. The local estimates of $A$, $B$, and $C$ allow determination of the expected maximum credible magnitude in a given time interval and the associated spread around ground shaking parameters (e.g., peak ground acceleration, PGA, or macroseismic intensity, $I_0$). Compilation of the corresponding seismic hazard map of Altai–Sayan Region and its rigorous testing against the available seismic evidences in the past is used to model regional maps of specific earthquake risks for population, cities, and infrastructures.

**Keywords** Unified scaling law for earthquakes · Earthquake hazard · Seismic risk · Morphostructural zoning · Earthquake-prone node · Maximum credible earthquake

---

✉ Vladimir G. Kossobokov
volodya@mitp.ru

[1] Institute of Earthquake Prediction Theory and Mathematical Geophysics, RAS, Moscow, Russian Federation

[2] Geophysical Center, RAS, Moscow, Russian Federation

[3] International Seismic Safety Organization, Arsita, Italy

# 1 Introduction

Earthquakes are complex natural phenomena associated with the dynamics of lithospheric blocks of all sizes, the accumulation and discharge of tectonic stress (Keilis-Borok 1990). Strongest earthquakes and inflicted phenomena, like landslides, tsunami, liquefactions, etc., occur suddenly and, occasionally, lead to serious economic consequences and casualties. Reducing the effects of natural disasters is a complex scientific and technical problem of great social and economic importance. Its relevance is continuously growing due to the increase of population and infrastructure densities, increasing anthropogenic impact on the ecology, the development of environmentally hazardous industries, etc.

Practice shows that the traditional probabilistic seismic hazard assessment techniques are not able to reliably characterize the real danger to the object at risk of a catastrophic earthquake (Kossobokov and Nekrasova 2010, 2012; Geller 2011; Wyss et al. 2012; Panza et al. 2014; Nekrasova et al. 2014; Kossobokov et al. 2015) because, locally, strong earthquakes occur very rarely so that their number is not enough for justifiable statistics. However, in general these events in particular determine most of the enormous total damage caused by earthquakes and cascading catastrophes. Thus, the development of state-of-the-art methods for adequately evaluating and reliable assessment of seismic hazard and risks is one of the main directions aimed at solving the itchy problem of reducing losses from natural disasters (Panza et al. 2011).

The widespread probabilistic maps (Giardini et al. 1999) are shown to be ineffective in practice, leading to an unexpected tremendous damage arising from earthquakes and cascading effects, as well as from considerable unnecessary costs for resistance in places where strong earthquakes or inflicted phenomena are impossible (Castaños and Lomnitz 2002; Klügel 2007; Geller 2011; Wang 2011; Kossobokov and Nekrasova 2012; Wyss et al. 2012; Wyss 2015). We keep contributing to the necessary urgent replacement of the existing customary probabilistic seismic hazard assessment maps that define the national building codes and regulations in Russian Federation and other countries (Peresan et al. 2013; Parvez et al. 2014; Nekrasova et al. 2014, 2015; Nekrasova and Kosobokov 2016; Parvez et al. 2017). In contrast to the use of the Global Seismic Hazard Assessment Program (GSHAP) methodology (Cornell 1968; Giardini et al. 2003), we have proposed replacing the subjective choice of a relatively small number of foci of strong earthquakes by an objective systematic analysis of the entire seismic evidence in the study area based on Unified Scaling Law for Earthquakes (USLE), pattern recognition of the earthquake-prone sites based on structural geomorphic zonation parameters (Gelfand et al. 1976; Gvishiani et al. 1986; Gorshkov et al. 2003), and neo-deterministic seismic hazard assessment based on seismic wave propagation in laterally heterogeneous anelastic media (Panza et al. 2001, 2012; Peresan et al. 2011).

# 2 Methodology

We apply the same methodology of seismic hazard and risks estimation (Parvez et al. 2014, 2017; Panza et al. 2014; Nekrasova et al. 2015) based on USLE which generalizes the Gutenberg–Richter relationship accounting for apparently fractal distribution of epicenters in the following form (Kossobokov and Mazhkenov 1994; Nekrasova and Kossobokov 2002, 2005, 2006):

$$\log_{10} N(M, L) = A + B \cdot (5-M) + C \cdot \log_{10} L \tag{1}$$

where $N (M, L)$ is the expected annual number of earthquakes of a certain magnitude M within an seismically prone area of linear dimension $L$; the constants $A$ and $B$ are analogous to $a$ and $b$ of the Gutenberg–Richter relationship, and the constant $C$ specifies the local fractal dimension of the earthquake epicenter loci. The constants $A$, $B$, and $C$ are obtained by application of the algorithm for Scaling Coefficients Estimation, named SCE and thoroughly described in (Nekrasova et al. 2011, 2015).

In assessment of seismic hazard the coefficients $A$, $B$, and $C$ are determined at the grid points predetermined by the nodes of morphostructural zoning (Gorshkov et al. 2003) or the empirical distribution of epicenters or the regular net then used to estimate the expected magnitude of Maximum Credible Earthquake, MCE. Specifically, to comply with a traditional 10% chance of exceedance in 50 years, for each $0.25° \times 0.25°$ cell centered at a grid point $c$ we calculate the expected number of earthquakes from the magnitude range $Mj$ in 50 years, then find the maximum magnitude, $M$max, with the expected number $50 \times N$ ($M$max, $0.25°$) $\geq$ 10%. The achieved values of $M$max at the entire set of grid points $\{c\}$ are used to determine seismic hazard in the region considered in terms of a selected ground shaking effect like macroseismic intensity, peak ground acceleration, etc. This could be obtained by applying neo-deterministic earthquake scenario modeling (Panza et al. 2001, 2012; Peresan et al., 2011) or, for an admissible simpler model assessment, the empirical formulae. In this study we consider the peak ground acceleration, PGA, and apply, at each point $s$ of a regular grid covering the entire Altai–Sayan region, the empirical formula as inspired from (Parvez et al. 2001, 2003), i.e.,

$$\text{Acc}_s\left(M\max_c\right) = \text{const} \times g \times D_{sc} - 1.5 \times \exp\left(M\max_c - 5\right) \tag{2}$$

where $D_{sc}$ is the source-receiver distance from $s$ to $c$ on a $0.25° \times 0.25°$ grid (we opt the minimum and maximum distances of 10 km and 500 km, respectively), const = 6, $g = 9.81$ m/s$^2$ is the gravity constant, $M$max$_c$ is the $M$max value at site $c$, and exp($X$) is the natural exponent of $X$. The maximum of acceleration values computed at a grid point $s$ of the regular grid is assigned to it, i.e., –

$$H(s) = PGA(s) = \max\left(\text{Acc}_s\left(M\max_c\right), c \text{ from } \{c\}\right) \tag{3}$$

In assessment of seismic risks, one may face many different risk estimates even if the same object of risk is considered. Specifically, it may result from the different laws of convolution, as well as from different kinds of vulnerability of an object of risk under specific environments and conditions. The conceptual issues must be resolved in a multidisciplinary problem-oriented study by specialists in the fields of hazard, objects of risk, and object vulnerability. To illustrate this concept, we consider the oversimplified risk $R(x)$ being the product of seismic hazard assessment $H(x)$ and vulnerable population, i.e., –

$$R(x) = H(x) \cdot \int_x P \cdot f(P) \tag{4}$$

where $\int_x P$ is the integral of the population density P over the cell $x$, i.e., the number of individuals within the area of the cell $x$, and $f(P)$ is the vulnerability of an individual as a function of $P$. For example, one may set individual vulnerability in proportion to some power of the population density, which appears to characterize the specifics of man-made environment in the areas of high concentration of individuals. A comparative analysis of

such risk estimates are given in (Parvez et al. 2014; Nekrasova et al. 2015; Nekrasova and Kosobokov 2016).

# 3 Data

The following seismic and population data for Altai–Sayan Region within 46°–56°N and 82°–99°E (Fig. 1) are used in the assessment of earthquake related hazard and risks.

## 3.1 Seismic data

The regional catalog is compiled using the annual periodicals "*The earthquakes of Northern Eurasia*" in 1997–2009 and "*The earthquakes of Russia*" in 2003–2015 (see Starovoit 2015 and Malovichko 2017 and references therein to the earlier volumes). For Altai–Sayan Region, both periodicals provide the origin time and hypocenter location of seismic events and, as a rule, the energy class K officially adopted in the Soviet Union (Instruction 1982) along with exceptionally few determinations of magnitudes of different kind. The boundaries of Altai–Sayan Region are somewhat arbitrary, differing from each other and those in the regional catalog of strong earthquakes from ancient times through 1977 (Kondorskaya et al. 1982). However, in 1997–2015 the efficient determination of earthquake parameters within 46°–56°N and 82°–99°E (yellow outline in Fig. 1) appears to be rather stable and complete for seismic events above $K = 8$, which threshold corresponds to $M = 2.2$ according to the original definition by Rautian (1960): $K = 1.8 \cdot M + 4$. In addition to hardware re-equipment of the regional network after the 27 December 2011, $M_{wGCMT} = 6.7$ and 26 February 2012, $M_{wGCMT} = 6.6$ Tuva earthquakes, data processing has undergone significant changes, so that the traditional determination of K has been substituted in "*The earthquakes of Russia*" with a determination of magnitude ML, which correlation to the energy class estimates previously used in the region has not been
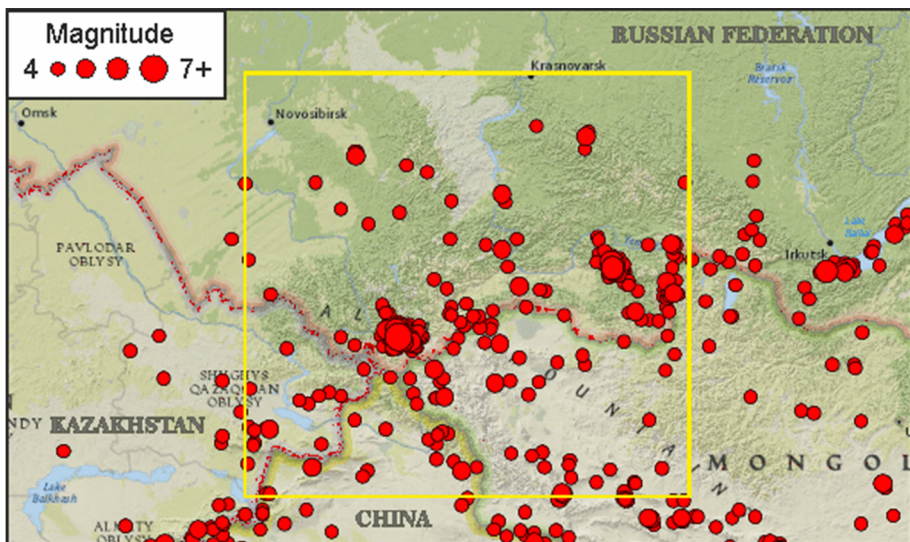


**Fig. 1** Magnitude 4 or greater earthquakes nearby Altai–Sayan Region, 1997–2015

sufficiently studied (Malovichko 2015). In our study, we use the magnitude scale $M = (K - 4)/1.8$ based on the traditional determination of K taking a liberty of calibrating ML to the earlier standards of regional magnitude M. The plots of magnitude determinations by the origin time (Fig. 2) in "*The earthquakes of Northern Eurasia*" (red), "*The earthquakes of Russia*" (blue), its supplementary data (green), and readjusted data in 2014–2015 (violet) show apparent irregularity in publication of seismic data recorded in the region. In particular, the catalog in 2012 is evidently incomplete without a supplementary sample of aftershocks of the two strong Tuva earthquakes. The calibrated catalog without duplicates contains 10,685 earthquakes of magnitude 2 or larger. The Gutenberg–Richter frequency–magnitude plots (Fig. 3) confirm reasonable completeness of the calibrated catalog above magnitude $M = 2.5$ and indicate the overcritical state of seismic activity in the region by the apparent excessive number of magnitude 6.5 or larger events. In addition to 19 years of the comprehensive regional catalog, the historical record of earthquakes from ancient times (Kondorskaya et al. 1982) is available for characterizing local seismic hazard in Altai–Sayan Region. The list of strong, magnitude 6 or larger earthquakes since 1734 to the present is given in Table 1.

### 3.2 Population data

The population data are taken from Gridded Population of the World (2005) that is a raster data product compiled at Center for International Earth Science Information Network (CIESIN), Columbia University, and Centro Internacional de Agricultura Tropical (CIAT). These population density distribution maps of the region based on the GPWv3 estimate for 2015 on the $0.25° \times 0.25°$ grid are given in Fig. 4. In addition, we use the data available from (Federal State Statistics Service 2016) to characterize seismic risks for the cities with population above 100,000 inhabitants in Altai–Sayan Region.

### 3.3 Morphostructural nodes

Morphostructural zoning (MSZ) has been initially designed by Gerasimov and Rantsman (1973) with a special aim for identifying earthquake-prone areas. Gelfand et al. (1972) pioneered applying pattern recognition in conjunction with MSZ to the Pamirs and Tien Shan, then to California and Nevada (Gelfand et al. 1976). The successful performance in recognition of the areas prone to large earthquakes in advance of their occurrence including the places without any historical record of such event in the past is described in (Gorshkov et al. 2003; Soloviev et al. 2014). The MSZ map of Altai–Sayan Region and Baikal (Fig. 5) is compiled recently by Gorshkov et al. (2018) based on the same principles and, presumably, with the same accuracy of identification of morphostructural nodes prone to
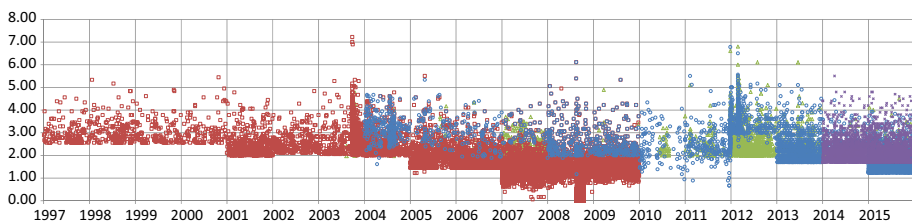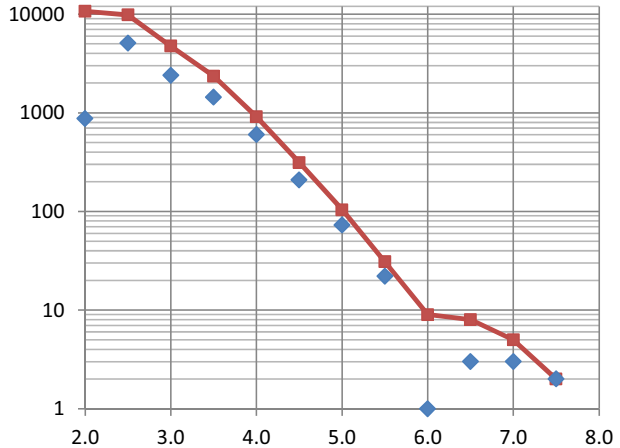


**Fig. 2** Earthquake magnitude plot for Altai–Sayan Region, 1997–2015

**Fig. 3** The Gutenberg–Richter incremental (blue diamonds) and cumulative (red) frequency-magnitude plots: Altai–Sayan Region, 1997–2015



magnitude 6.0 or larger earthquakes. Thus, in the following application of the USLE-based approach to SHA in Altai–Sayan Region we consider all 63 intersections of the MSZ lineaments including the 19 of those recognized as prone to strong earthquakes (i.e., yellow circles within the region boundary in blue).

## 4 Application of the SCE algorithm

The SCE algorithm was applied to the calibrated catalog of earthquakes defined in Sect. 3.1. It considered the hierarchy of square boxes with linear size of 2°, 1°, 1/2°, and 1/4° centered at grid points of three types, i.e., (1) the grid points of the regular 1/4° × 1/4° with 2 or more earthquakes from the calibrated catalog in its 1/4° × 1/4° cell (Fig. 6), (2) the grid points with a historical strong earthquake (Table 1) in its cell, and (3) each node of the MSZ map. Reliable estimates of coefficients A, B, and C are mapped in Fig. 7 along with the squared sum of their standard errors $\sigma_A$, $\sigma_B$, and $\sigma_C$. The error of determination of the USLE coefficients at 204 out of 207 nodes does not exceed 0.01, which confirms rather high quality of the mapped values for the entire territory Altai–Sayan Region.

The distribution of the level of seismic activity (coefficient A) has the three characteristic maxima, of which the two largest at A about − 0.3 and − 0.6 correspond to the expectation of one earthquake with M = 5.0 in about 2 and 4 years, respectively. The third local maximum at A = − 1.4 corresponds to once in about 25 years and appears to be the median of recurrences in range from one in 10 to one in more than 60 years. Most of the B values, which characterize the slope of the frequency–magnitude graph, vary from 0.6 to 1.0 with the sharp peak at 0.95. The estimates of B below 0.6 in Mongolia are related to local incompleteness of the calibrated catalog due to deficiency of the regional seismographic stations. The fractal dimension of distributed epicentres C varies broadly from below 0.6 to above 1.4 following a bi-modal shape with a pronounced peak about 0.7 and a plateau from 1.1 to 1.3. The first generally corresponds to the clusters of activity on the morphostructural lineaments of the Altai Mountains and Eastern Sayan and the second—to the most fractured areas in between those, where the values of C > 1.2 are in common.

**Table 1** The magnitude 6 or larger earthquakes from ancient times to the present within 46°–56°N and 82°–99°E

| Year | Month | Day | Hour | Minute | Second | Latitude, °N | Longitude, °E | Depth, km | M | Catalogue |
|---|---|---|---|---|---|---|---|---|---|---|
| 1761 | 12 | 9 | 17 | 20 | – | 50.00 | 90.00 | 30 | 7.7 | [1] |
| 1771 | 3 | 1 | 2 | – | – | 51.00 | 99.00 | 30 | 6.0 | [1] |
| 1857 | 12 | 24 | 7 | 50 | – | 48.30 | 83.40 | 24 | 6.4 | [1] |
| 1902 | 12 | 28 | 1 | 43 | 19 | 50.70 | 91.30 | 30 | 6.6 | [1] |
| 1903 | 3 | 12 | 14 | 19 | – | 53.90 | 87.00 | 30 | 6.1 | [1] |
| 1905 | 3 | 15 | 17 | 55 | – | 52.70 | 92.60 | 30 | 6.1 | [1] |
| 1905 | 7 | 9 | 9 | 40 | 39 | 49.71 | 98.48 | 15 | 8.3 | [2] |
| 1905 | 7 | 9 | 10 | 57 | 24 | 49.50 | 97.30 | 20 | 6.7 | [1] |
| 1905 | 7 | 9 | 11 | 21 | 21 | 49.50 | 97.30 | 20 | 6.8 | [1] |
| 1905 | 7 | 11 | 8 | 38 | – | 49.50 | 97.30 | 20 | 7.0 | [1] |
| 1905 | 7 | 14 | 22 | 1 | – | 49.50 | 97.30 | 20 | 6.5 | [1] |
| 1905 | 7 | 16 | 18 | 52 | – | 51.70 | 90.20 | 20 | 6.0 | [1] |
| 1905 | 7 | 23 | 2 | 46 | 22 | 49.37 | 96.61 | 15 | 8.3 | [2] |
| 1905 | 7 | 23 | 4 | 18 | – | 49.30 | 96.20 | 20 | 6.4 | [1] |
| 1905 | 7 | 23 | 20 | 35 | – | 49.30 | 96.20 | 20 | 6.0 | [1] |
| 1905 | 9 | 1 | 2 | 48 | – | 49.30 | 96.20 | 20 | 6.1 | [1] |
| 1917 | 11 | 28 | 14 | 42 | 44 | 46.90 | 89.00 | 20 | 6.1 | [1] |
| 1922 | 8 | 25 | 19 | 29 | 45 | 50.04 | 90.85 | 10 | 6.6 | [2] |
| 1923 | 9 | 14 | 12 | 57 | 31 | 48.00 | 96.00 | 11 | 6.0 | [1] |
| 1923 | 9 | 21 | 20 | 1 | 21 | 49.80 | 87.70 | 8 | 6.0 | [1] |
| 1927 | 4 | 21 | 3 | 21 | 20 | 50.20 | 86.90 | 28 | 6.0 | [1] |
| 1931 | 8 | 10 | 21 | 18 | 30 | 46.50 | 90.50 | 40 | 7.8 | [1] |
| 1931 | 8 | 18 | 14 | 21 | – | 47.40 | 90.00 | 42 | 6.7 | [1] |
| 1931 | 11 | 5 | 12 | 19 | 30 | 47.00 | 90.00 | 20 | 6.3 | [1] |
| 1933 | 2 | 13 | 2 | 49 | 15 | 46.10 | 90.60 | 20 | 6.2 | [1] |
| 1938 | 10 | 19 | 4 | 13 | 30 | 49.11 | 89.71 | 10 | 7.1 | [2] |
| 1938 | 12 | 17 | 16 | 35 | 25 | 47.50 | 92.80 | 18 | 6.5 | [1] |
| 1970 | 5 | 15 | 17 | 13 | 13 | 50.22 | 91.12 | 7 | 6.3 | [2] |
| 1991 | 12 | 27 | 9 | 9 | 38 | 51.02 | 98.15 | 14 | 6.4 | [2] |
| 2003 | 9 | 27 | 11 | 33 | 25 | 50.04 | 87.81 | 16 | 7.3 | [2] |
| 2003 | 9 | 27 | 18 | 52 | 47 | 50.09 | 87.77 | 10 | 6.4 | [2] |
| 2003 | 10 | 1 | 1 | 3 | 25 | 50.21 | 87.72 | 10 | 6.7 | [2] |
| 2011 | 12 | 27 | 15 | 21 | 57 | 51.84 | 95.91 | 15 | 6.6 | [2] |
| 2012 | 2 | 26 | 6 | 17 | 20 | 51.71 | 95.99 | 12 | 6.7 | [2] |

[1] refer to (Kondorskaya et al. 1982); [2]—ANSS Comprehensive Earthquake Catalogue (https://earthquake.usgs.gov/earthquakes/search/ last visited on 18 September 2017)
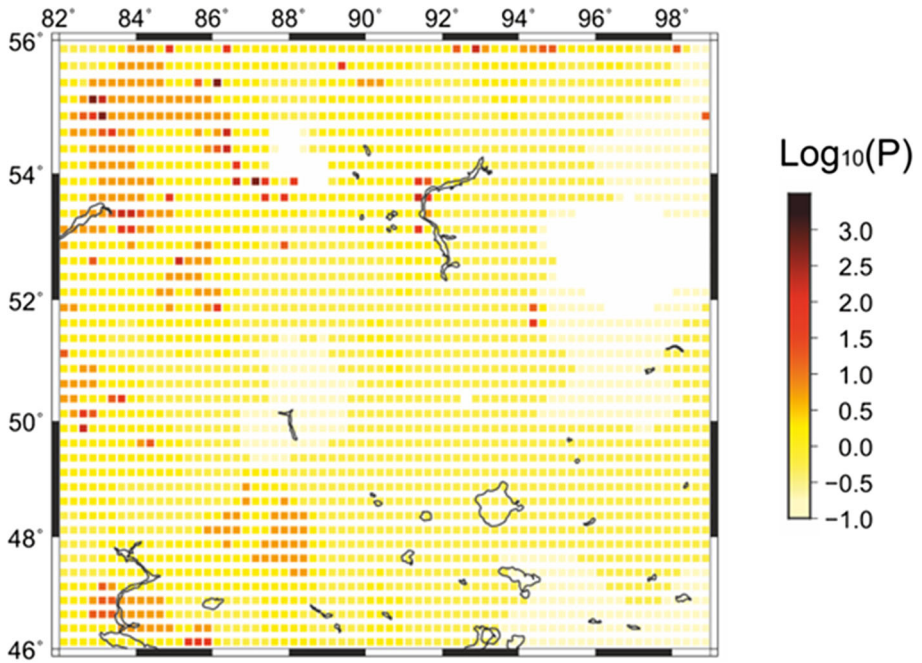
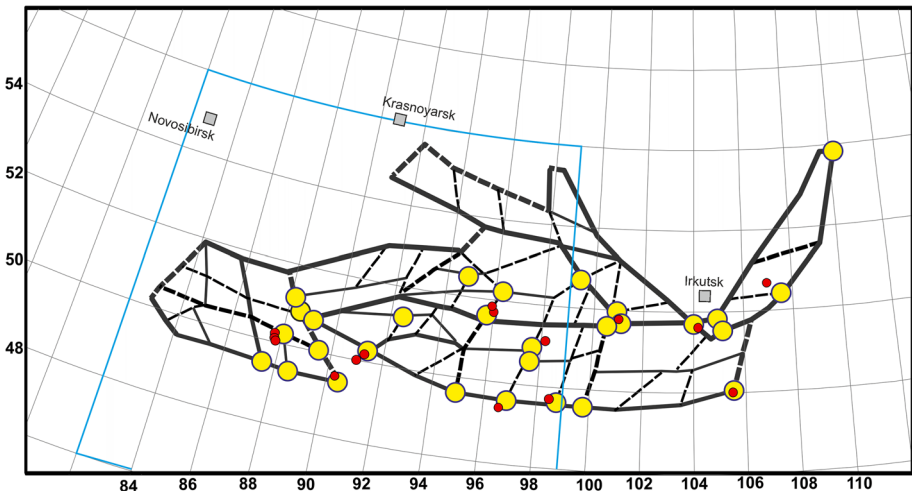**Fig. 4** The population density $P$ (in ind/km$^2$): The GPWv3 estimate for the year 2015



**Fig. 5** The MSZ map of Altai–Baikal Region (after Gorshkov et al. 2018). *Note* The yellow circles indicate the MSZ nodes recognized as prone to strong earthquakes ($M \geq 6$) by the Cora-3 algorithm (Gelfand et al. 1976). The epicentres of magnitude $M \geq 6$ earthquakes are marked with red dots. The blue line is the boundary of Altai–Sayan Region considered in this study
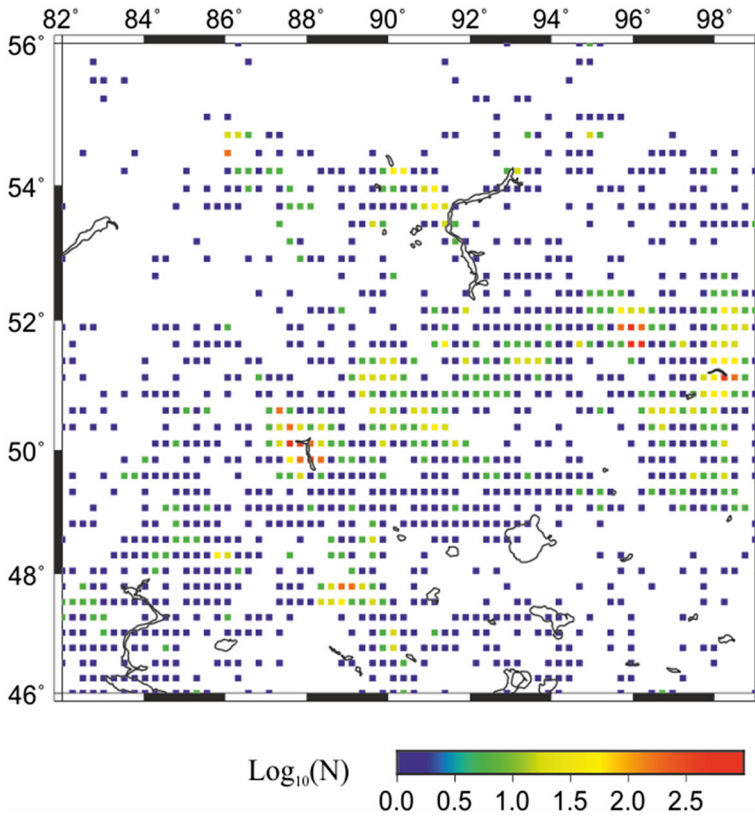
**Fig. 6** The number of earthquakes of magnitude $M = 2.78$ or larger in Altai–Sayan Region, 1997–2015

## 5 Hazard and risk determination

The values of the USLE coefficients at the 207 grid points were used to determine the distribution of the magnitude of the MCE events mapped in Fig. 8c. In addition to the USLE prediction of expected location of MCE's, we used the recent pattern recognition results by Gorshkov et al. (2018) and the historical maximum of earthquake magnitude in 1734–2017 (Fig. 8a, b, respectively). The combined map of *Mmax* (Fig. 8d) is used in calculation of seismic hazard, in terms of PGA with 10% of exceedance in 50 years, for the entire territory of Altai–Sayan Region which is mapped in Fig. 9a. Figure 9b shows the GSHAP PGA map (Giardini et al. 1999) for the same territory. The two maps differ dramatically.

To illustrate the complexity of seismic risk assessment, we calculated and plotted in Fig. 10 the maps of $R_i(s) = H(s) \cdot \int_s P$, $R_{ii}(s) = H(s) \cdot \int_s P \cdot P$, $R_{iii}(s) = H(s) \cdot \int_s P \cdot P^2$, and $R_{iv}(s) = H(s) \cdot \int_s P \cdot P^3$ where individual vulnerability is proportional to the power 0, 1, 2, and 3 of the population density, correspondingly (Fig. 10). The model risk estimates are derived from the seismic hazard maps given in Fig. 9. For each map, the risk is given in arbitrary units proportional to the maximum value set to 1000. The color of a cell corresponds to the decimal logarithmic scale in range from 1000 to 0.01. Figure 11 displays for a comparison the empirical distributions of the four model risks in Altai–Sayan Region.
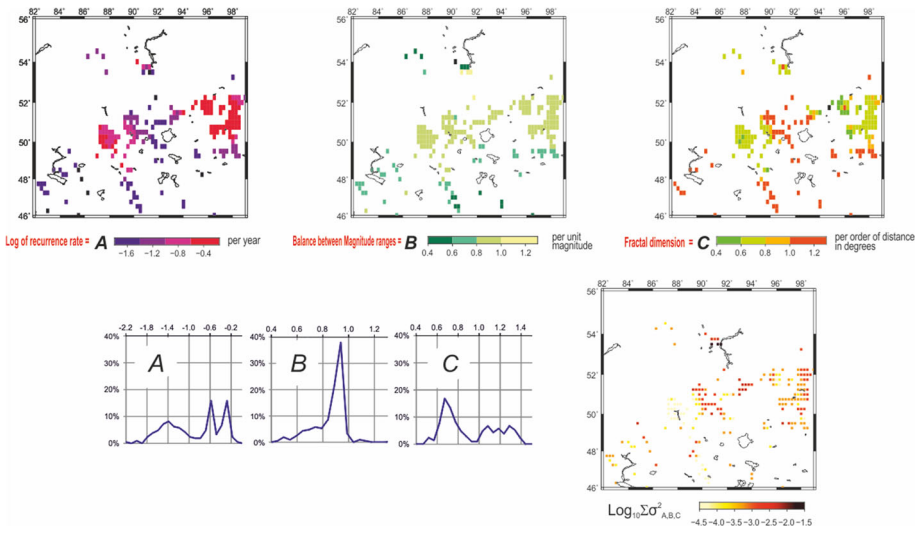
**Fig. 7** The regional maps of A, B, and C coefficients (upper row), their empirical probability density distribution functions and the regional map distribution of the sum of errors $\sum \sigma^2 = \sigma_A^2 + \sigma_B^2 + \sigma_C^2$ (bottom row)
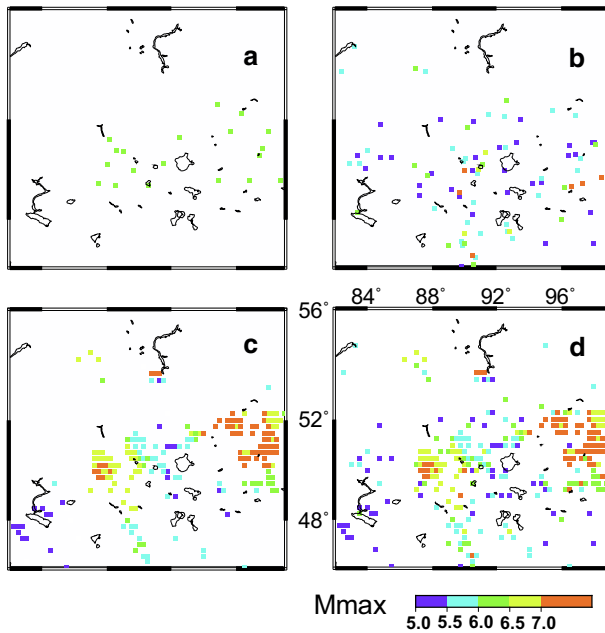


**Fig. 8** The seismic hazard map for the region in terms of $M_{max}$ at earthquake-prone cells of the regular $0.25° \times 0.25°$ grid: **a** the MSZ nodes recognized as prone to magnitude 6 or larger earthquakes; **b** the maximum of observed magnitude in 1734–2017 from (Kondorskaya et al. 1982) and the USGS ANSS Comprehensive Earthquake Catalogue (https://earthquake.usgs.gov/earthquakes/search/—last visited on 18 September 2017); **c** the maximum magnitude expected with 10% chance in 50 years based on the SCE algorithm computations; **d** the combined map of $M_{max}$
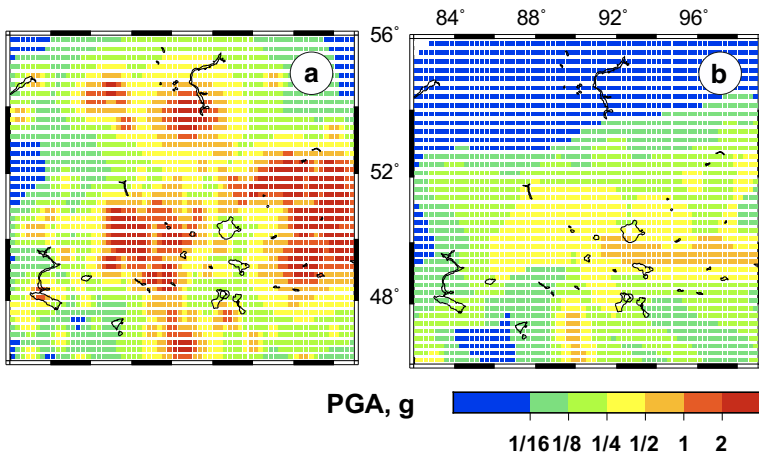
**Fig. 9** The seismic hazard maps for Altai–Sayan Region in terms of expected peak ground acceleration, PGA, with 10% chance of exceedance in 50 years: **a** this study; **b** the probabilistic GSHAP map. (Reproduced with permission from Giardini et al. 1999)
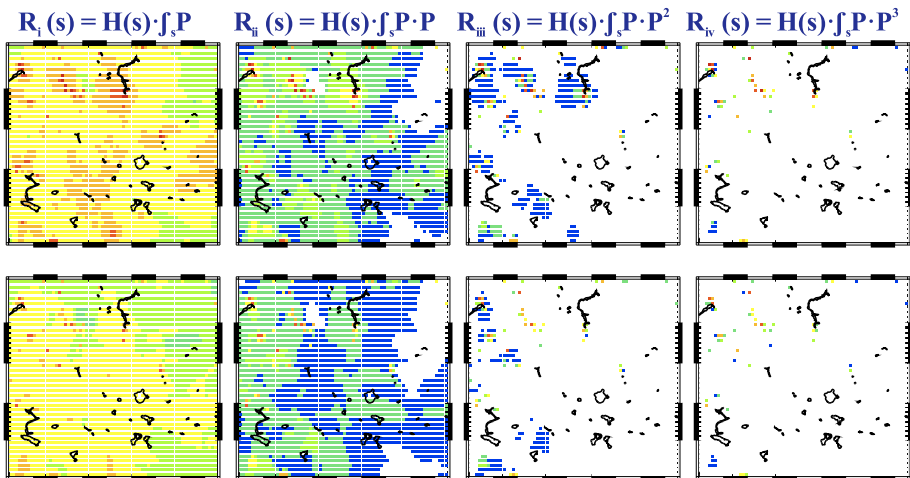


**Fig. 10** The maps of the model seismic risks $R_{\mathrm{i}}$, $R_{\mathrm{ii}}$, $R_{\mathrm{iii}}$, and $R_{\mathrm{iv}}$ for population of Altai–Sayan Region based on the hazard maps of this study (upper row) and GSHAP (bottom row). *Note* each risk scale is given in arbitrary units with the maximum of the expected values in the region set to 1000

Evidently, the USLE-based risk estimates are larger. Naturally, the maximum risk for population is concentrated at the urban agglomerations and drops dramatically when moving to the rural districts and uninhabited territories.

Table 2 summarizes the results of seismic hazard and risk estimates for the 11 cities with population above 100,000 inhabitants affected by earthquakes in Altai–Sayan Region. The top 2 values of Population, city area $S$, and PGA given in bold disclose the complex combinations of possibilities. For example, the most populated city of Novosibirsk is among the lowest in respect to the seismic hazard based on GSHAP, while being the 4th largest based on USLE; the city of Kyzyl of the smallest area is the 1st and 2nd most
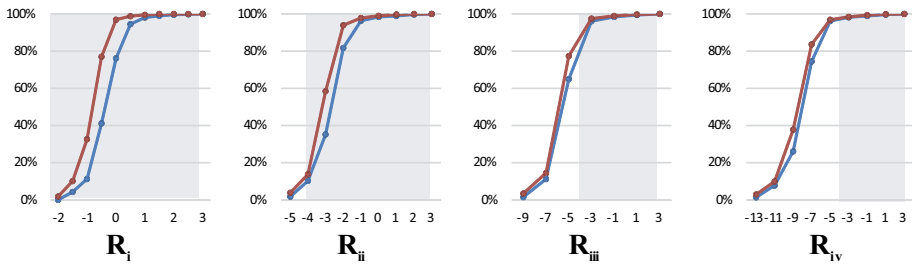
**Fig. 11** The empirical probability distributions of the model seismic risks $R_i$, $R_{ii}$, $R_{iii}$, and $R_{iv}$ for population of Altai–Sayan Region based on the hazard maps of this study (blue) and GSHAP (red). Note: the gray background marks the range of seven decimal orders of risk shown in Fig. 10

| | City | $P$ | $S$, km$^2$ | PGA, g | | Ratio |
|---|---|---|---|---|---|---|
| | | | | GSHAP | This study | |
| **Table 2** Seismic hazard at the principal cities of Altai–Sayan Region | Abakan | 165,214 | 112.4 | 0.06 | **5.74** | **95.86** |
| | Achinsk | 109,155 | 103.0 | 0.02 | 0.15 | **7.80** |
| | Barnaul | 612,401 | 321.0 | 0.04 | 0.07 | 1.55 |
| | Biysk | 210,115 | 291.7 | **0.10** | 0.09 | 0.88 |
| | Kemerovo | 532,981 | 282.3 | 0.02 | 0.16 | **7.85** |
| | Krasnoyarsk | **1,083,865** | 348.0 | 0.02 | 0.14 | **6.04** |
| | Kyzyl | 109,918 | 97.4 | **0.20** | **3.97** | **19.41** |
| | Novokuznetsk | 547,904 | 424.3 | 0.05 | 0.61 | **11.89** |
| | Novosibirsk | **1,602,915** | **505.6** | 0.02 | 0.29 | **11.71** |
| | Oskemen[a] | 321,251 | **540.0** | 0.06 | 0.24 | **4.27** |
| [a]Oskemen (Kazakhstan) is also known as Ust-Kamenogorsk | Tomsk | 524,669 | 297.2 | 0.02 | 0.07 | 3.32 |

seismically hazardous for GSHAP and USLE approaches, respectively. Note that the ratio of the two hazard estimates, PGA$_{USLE}$/PGA$_{GSHAP}$ (Table 2, last column), discloses unacceptable underestimation of seismic hazard (by factor 4 or greater) in 8 out of 11 significant cities of Altai–Sayan Region. The GSHAP and USLE-based estimates of the four risks for the eleven significant cities in the region are given in Table 3. For each of the four risks, their values are given in proportion to the maximum of the GSHAP and USLE estimates set at 1000; those in the top decimal order are highlighted. All of them, i.e., 5, 6, 5, and 3, belong to the $R_i$, $R_{ii}$, $R_{iii}$, and $R_{iv}$ estimates based on USLE approach, correspondingly. (For an obvious reason the ratio of the GSHAP and USLE-based estimates of risks is the same as for the seismic hazard estimates in Table 2.) We observe the change in the order of most risky cities: e.g., the city of Abakan, the most risky in terms of $R_i$ is the 2nd in terms of $R_{ii}$ and $R_{iii}$ and the 3rd in terms of $R_{iv}$; the city of Novosibirsk is the 2nd in terms of $R_i$ becomes the most risky when any of the other three kinds of risk is considered.

Let us emphasize that our estimates of seismic hazard and risks for Altai–Sayan Region are presented for academic purposes highlighting the general problem-oriented approach based on USLE. Evidently, these estimates do not use more adequate though complicated procedures of convolutions of seismic hazard, objects of risks, and their vulnerability. The studies addressing realistic and practical kinds of seismic risks should bring together

**Table 3** The 4 seismic risks for the principal cities of Altai–Sayan Region

| City | $R_i$ | | $R_{ii}$ | | $R_{iii}$ | | $R_{iv}$ | |
|---|---|---|---|---|---|---|---|---|
| | GSHAP | This study | GSHAP | This study | GSHAP | This study | GSHAP | This study |
| Abakan | 10.45 | **1000.00** | 9.89 | **945.86** | 4.58 | **438.54** | 2.13 | **203.32** |
| Achinsk | 2.30 | 17.27 | 1.57 | 11.77 | 0.52 | 3.94 | 0.18 | 1.32 |
| Barnaul | 25.83 | 45.20 | 31.71 | 55.49 | 19.08 | 33.39 | 11.48 | 20.10 |
| Biysk | 22.16 | 19.94 | 10.27 | 9.24 | 2.33 | 2.10 | 0.53 | 0.48 |
| Kemerovo | 11.24 | 89.92 | 13.66 | **109.25** | 8.13 | 65.06 | 4.84 | 38.74 |
| Krasnoyarsk | 22.86 | **160.01** | 45.81 | **320.69** | 45.01 | **315.05** | 44.22 | **309.51** |
| Kyzyl | 23.18 | **460.15** | 16.83 | **334.16** | 5.99 | **118.95** | 2.13 | 42.34 |
| Novokuznetsk | 28.89 | **352.43** | 24.00 | **292.86** | 9.78 | **119.28** | 3.98 | 48.59 |
| Novosibirsk | 33.81 | **490.17** | 68.97 | **1000.00** | 68.97 | **1000.00** | 68.97 | **1000.00** |
| Oskemen[a] | 20.33 | 81.30 | 7.78 | 31.12 | 1.46 | 5.84 | 0.27 | 1.10 |
| Tomsk | 11.07 | 38.73 | 12.57 | 44.00 | 7.00 | 24.50 | 3.90 | 13.64 |

[a]Oskemen (Kazakhstan) is also known as Ust-Kamenogorsk. The values of a risk are normalized to the maximum of GSHAP and USLE estimates set to 1000. The values above 100 are given in bold

seismologists and regional experts in earthquake engineering, social sciences, and economics.

# 6 Conclusions

The results of our investigation of seismic hazard and risks in Altai–Sayan Region are much more cautious and site specific than those of the Global Seismic Hazard Assessment Program (Giardini et al. 1999, 2003). It should be noted that the GSHAP PGA values are in contradiction to the seismic evidence worldwide (Kossobokov and Nekrasova 2010, 2012), which is avoided in our application of the USLE-based methodology in Altai–Sayan Region. In particular, the PGA values at epicenters of 131 earthquakes of magnitude 5.0 or larger in Altai–Sayan Region, 1761–2017, exceed the PGA values on the GSHAP map by factor of 2 or more in 52 cases. The ratio $PGA_{epi}/PGA_{GSHAP}$ exceeds 4 in 26 cases and—8 in 13 cases. For the 34 strong earthquakes of magnitude 6 or more from Table 1 the ratio exceeds 2 in 25 cases,—4 in 15 cases, and—8 in 8 cases. The GSHAP PGA at epicenters of all the seven significant earthquakes of magnitude 7 or greater is less than their $PGA_{epi}$ estimates by factor 2 or more; the ratio $PGA_{epi}/PGA_{GSHAP}$ exceeds 4 and for 6 earthquakes and 8 for 5 earthquakes. All this favors the USLE approach to the problem of assessing seismic hazard and risks.

Our study attempts to contribute modestly an urgent revision of the probabilistic seismic hazard maps by an improvement of background methodologies and implementation in assessment of seismic hazard and risks. Evidently, it does not take into consideration economic and social factors of risk assessment, neither accounts for the role of site effect due to topography and soils, nor makes use of an earthquake rupture size for the large and/ or complex seismic events. These essential considerations should be addressed in the future practical estimations and mappings.

# References

Castaños H, Lomnitz C (2002) PSHA: is it science? Eng Geol 66(3–4):315–317. https://doi.org/10.1016/S0013-7952(02)00039-X

Cornell CA (1968) Engineering seismic risk analysis. Bull Seismol Soc Am 58:1583–1606

Federal State Statistics Service (2016) The population of the Russian Federation for municipalities on January 1, 2016. FSSS: Moscow, Russian Federation. http://www.gks.ru/free_doc/doc_2016/bul_dr/mun_obr2016.rar. Assessed 19 Sept 2016

Gelfand IM, Guberman ShA, Izvekova ML, Keilis-Borok VI, Rantzman EYa (1972) On criteria of high seismicity. Trans (Doklady) Acad Sci SSSR 202:1317–1320

Gelfand IM, Guberman ShA, Keilis-Borok VI, Knopoff L, Press F, Ranzman EYa, Rotwain IM, Sadovsky AM (1976) Pattern recognition applied to earthquake epicenters in California. Phys Earth Planet Int 11:227–283

Geller RJ (2011) Shake-up time for Japanese seismology. Nature 472:407–409. https://doi.org/10.1038/nature10105

Gerasimov IP, Ranzman EYa (1973) Morphostructure of orogens and their seismicity. Geomorphology 1:3–13 (**in Russian**)

Giardini D, Grünthal G, Shedlock K, Zhang P (1999) The GSHAP global seismic hazard map. Ann Geofis 42(6):1225–1228

Giardini D, Grünthal G, Shedlock K, Zhang P (2003) The GSHAP global seismic hazard map. In: Lee WHK, Kanamori H, Jennings P, Kisslinger C (eds) International handbook of earthquake and engineering seismology, international geophysics series 81 B. Academic Press, Amsterdam, pp 1233–1239

Gorshkov A, Kossobokov V, Soloviev A (2003) Chapter 6. Recognition of earthquake-prone areas. In: Keilis-Borok VI, Soloviev AA (eds) Nonlinear dynamics of the lithosphere and earthquake prediction. Springer, Heidelberg, pp 239–310

Gorshkov AI, Soloviev AA, Zharkikh YuI (2018) Recognition of places of possible occurrence of strong earthquakes in the Altai–Sayan–Baikal region. Dokl Earth Sci 479(1):412–414. https://doi.org/10.1134/S1028334X1803025X

Gridded Population of the World, Version 3 (GPWv3) (2005) Palisades, NY: Socioeconomic Data and Applications Center (SEDAC), Columbia University, http://sedac.ciesin.columbia.edu/gpw. Accessed 05 July 2016

Gvishiani AD, Gorshkov AI, Kossobokov VG, Rantsman EYa (1986) Morphostructures and places of earthquaakes in the Greater Cousasus. Izvestia Acad Sci USSR Phys Earth 9:24–35 (**in Russian**)

Instruction on the order of production and processing of observations at seismic stations of the Unified System of Seismic Observations of the USSR (1982). Moscow, Nauka, p 273 (**in Russian**)

Keilis-Borok VI (1990) The lithosphere of the Earth as a nonlinear system with implications for earthquake prediction. Rev Geophys 28:19–34

Klügel JU (2007) Error inflation in probabilistic seismic hazard analysis. Eng Geol 90:186–192

Kondorskaya NV, Shebalin NV, Khrometskaya YaA, Gvishiani AD (1982) New catalog of strong earthquakes in the U.S.S.R. from ancient times through 1977. World data center a for solid earth geophysics, report SE-31, p 609

Kossobokov VG, Mazhkenov SA (1994) On similarity in the spatial distribution of seismicity. In: Chowdhury DK (ed) Computational seismology and geodynamics, vol 1. AGU, The Union, Washington DC, pp 6–15

Kossobokov V, Nekrasova A (2010) Global seismic hazard assessment program maps are misleading. Eos Trans AGU 91(52), Fall Meet Suppl, Abstract U13A-0020

Kossobokov V, Nekrasova A (2012) Global seismic hazard assessment program maps are erroneous. Seism Instrum 48(2):162–170. https://doi.org/10.3103/S0747923912020065

Kossobokov V, Peresan A, Panza GF (2015) Reality check: seismic hazard models you can trust. EOS 96(13):9–11

Malovichko AA (ed) (2015) The earthquakes of Russia in 2013. GS RAS, Obninsk, p 224 (**inc. CD-ROM**)

Malovichko AA (ed) (2017) The earthquakes of Russia in 2015. GS RAS, Obninsk, p 212 (**inc. CD-ROM**)

Nekrasova AK, Kosobokov VG (2005) Temporal variations in the parameters of the Unified Scaling Law for Earthquakes in the eastern part of Honshu Island (Japan). Dokl Earth Sci 405:1352–1356

Nekrasova AK, Kosobokov VG (2006) Unified scaling law for earthquakes in the Lake Baikal region. Dokl Earth Sci 407A(3):484–485

Nekrasova AK, Kosobokov VG (2016) Unified scaling law for earthquakes in crimea and Northern Caucasus. Dokl Earth Sci 470(2):1056–1058

Nekrasova A, Kossobokov V (2002) Generalizing the Gutenberg–Richter scaling law. EOS Trans AGU 83(47), NG62B–0958

Nekrasova A, Kossobokov V, Perezan A, Aoudia A, Panza GF (2011) A multiscale application of the unified scaling law for earthquakes in the central mediterranean area and Alpine region. Pure appl Geophys 168:297–327. https://doi.org/10.1007/s00024-010-0163-4

Nekrasova A, Peresan A, Kossobokov VG, Panza GF (2014) Chapter 7: a new probabilistic shift away from seismic hazard reality in Italy? In: Aneva B, Kouteva-Guentcheva M (eds) Nonlinear mathematical physics and natural hazards, Springer Proceedings in Physics, vol 163, pp 83–103. http://dx.doi.org/10.1007/978-3-319-14328-6_7

Nekrasova A, Kossobokov V, Parvez IA, Tao X (2015) Seismic hazard and risk assessment based on the unified scaling law for earthquakes. Acta Geod Geophys 50(1):21–37. https://doi.org/10.1007/s40328-014-0082-4

Panza GF, Romanelli F, Vaccari F (2001) Seismic wave propagation in laterally heterogeneous anelastic media: theory and applications to seismic zonation. Adv Geophys 43:1–95

Panza G, Irikura K, Kouteva-Guentcheva M, Peresan A, Wang Z, Saragoni R (eds) (2011) Advanced seismic hazard assessment. Pure Appl Geophys, vol 168 (1–4), p 752

Panza GF, La Mura C, Peresan A, Romanelli F, Vaccari F (2012) Seismic hazard scenarios as preventive tools for a disaster resilient society. In: Dmowska R (ed) Advances in geophysics. Elsevier, London, pp 93–165

Panza GF, Kossobokov V, Peresan A, Nekrasova A (2014) Chapter 12. Why are the standard probabilistic methods of estimating seismic hazard and risks too often wrong? In: Wyss M, Shroder J (eds) Earthquake hazard, risk, and disasters. Elsevier, London, pp 309–357

Parvez IA, Gusev A, Panza GF, Petukhin A (2001) Preliminary determination of the interdependence among strong motion amplitude, earthquake magnitude and hypocentral distance for the Himalayan region. Geophys J Int 144:577–596

Parvez IA, Vaccari F, Panza GF (2003) A deterministic seismic hazard map of India and adjacent areas. Geophys J Int 155:489–508

Parvez IA, Nekrasova A, Kossobokov V (2014) Estimation of seismic hazard and risks for the Himalayas and surrounding regions based on unified scaling law for earthquakes. Nat Hazards 71(1):549–562. https://doi.org/10.1007/s11069-013-0926-1

Parvez IA, Nekrasova A, Kossobokov V (2017) Earthquake hazard and risk assessment based on unified scaling law for earthquakes: state of Gujarat, India. Pure Appl Geophys 174(3):1441–1452. https://doi.org/10.1007/s00024-017-1475-4

Peresan A, Zuccolo E, Vaccari F, Gorshkov A, Panza GF (2011) Neo-deterministic seismic hazard and pattern recognition techniques: time-dependent scenarios for North-Eastern Italy. Pure appl Geophys 168(3):583–607. https://doi.org/10.1007/s00024-010-0166-1

Peresan A, Magrin A, Nekrasova A, Kossobokov VG, Panza GF (2013) Earthquake recurrence and seismic hazard assessment: a comparative analysis over the Italian territory. In: Proceedings of the ERES 2013 conference. WIT Transactions on the Built Environment, vol 132, pp 23–34. http://dx.doi.org/10.2495/ERES130031

Rautian TG (1960) Energy of earthquakes. In: Methods of detailed study of seismicity. Moscow: Publishing house of the Institute of Physics of the Academy of Sciences of the USSR, pp 75–114. (Trudy IFZ AN SSSR, No. 9 (176))

Soloviev AA, Gvishiani AD, Gorshkov AI, Dobrovolsky MN, Novikova OV (2014) Recognition of earthquake prone areas: methodology and analysis of the results. Izv Phys Solid Earth 50(2):151–168

Starovoit OE (ed) (2015) The earthquakes of Northern Eurasia, 2009. FSIS GS RAS, Obninsk, p 394 **(inc. CD-ROM)**

Wang ZM (2011) Seismic hazard assessment: issues and alternatives. Pure appl Geophys 168(1–2):11–25. https://doi.org/10.1007/s00024-010-0148-3

Wyss M (2015) Chapter 20: do probabilistic seismic hazard maps address the need of the population? In: Wyss M, Peppoloni S (eds) Geoethics: ethical challenges and case studies in earth sciences. Elsevier, New York, pp 239–249. https://doi.org/10.1016/B978-0-12-799935-7.00020-4

Wyss M, Nekrasova A, Kossobokov V (2012) Errors in expected human losses due to incorrect seismic hazard estimates. Nat Hazards 62(3):927–935. https://doi.org/10.1007/s11069-012-0125-5